Spectral Correction for the Effect of Crown Shape at the Single-Tree Level: An Approach Using a Lidar-Derived Digital Surface Model for Broad-Leaved Canopy

Youngkeun Song, *Member, IEEE*, Junichi Imanishi, Hiroshi Hashimoto, Atsuo Morimura, Yukihiro Morimoto, and Katsunori Kitada

***Abstract*—The spectral response of a single tree on remotely sensed images may be affected by the crown shape, yielding brighter sun-facing sides and darker sides facing away from the sun. To correct this crown-shape effect, we assumed that the roughness of the canopy surface within a single crown resembles the topography of the land surface, in the case of a closed upper-canopy layer (i.e., canopy surface) of broad-leaved deciduous trees. Previous topographic normalizations have proved to be useful in correcting the effect of rugged terrain at a large-landscape scale. However, are they also useful in correcting the rough canopy surface at the scale of a single crown? We applied conventional topographic corrections (cosine, Minnaert, and C) to a canopy surface model (CSM) of 66 trees, which was derived from airborne small-footprint Lidar data. The 12-band spectral data of each tree were acquired from the aircraft with 0.5-m spatial resolution and analyzed to validate the corrections. Among the tested methods, the C correction was the most successful in applying to the CSM, whereas the Minnaert and cosine corrections yielded errors in the reflectance of some steep canopy surfaces. We assessed the spectral feature of each tree in terms of tree vigor, by using the vegetation index employing the red-edge (700 nm) and green (541 nm) bands. Following the correction, the overall accuracy was improved from 75.5% to 84.5%. Thus, we suggest that the effect of crown shape be carefully considered and corrected in single-crown-level analyses of remotely sensed spectra.**

***Index Terms*—Airborne remote sensing, canopy surface model (CSM), closed canopy, crown condition, topographic correction.**

I. Introduction

THE CROWN shape of a tree is a critical parameter in determining the canopy reflectance [1]. This point has been emphasized in geometric optical modeling approaches [1]–[4], which attempted to treat the canopy as an assemblage of solid 3-D objects. The objects (i.e., trees) were fixed in the model as cones [2], [3] or spheres [4], [5] for discrete coniferous or shrub canopies, respectively. However, in a closed canopy of broad-leaved deciduous trees, the morphological assumption of regular crown shape may be far from valid. Accordingly, the crown shape of a broad-leaved deciduous tree should be considered based on more realistic measurements.

In terms of modeling the crown-shape effect, the approach taken to topography may be useful. Rugged terrain has a strong influence on radiance in remote sensing images. Because radiance varies with slope orientation and angle, a surface appears to be darker when facing away from the sun and brighter when facing the sun. This slope-aspect effect, or topographic effect, has been recognized when classifying forest type [6]–[11] and predicting the biophysical parameters of a forest [12], [13]. Our understanding of the topographic effect on remote sensing imagery can be applied to the case of tree-crown shape. The shape of upper tree crowns [14] (i.e., the canopy surface) at the scale of a single crown can be compared with that of mountains at a regional scale, particularly regarding the closed upper-canopy layer of broad-leaved deciduous trees. The roughness of canopy surface may generate the same influences on canopy reflectance as those resulting from mountainous terrain [15]. In recent years, remote sensing has observed a single tree as dozens of pixels, meaning that the pixels within a single crown may be affected by the roughness of the tree canopy, i.e., they may appear to be brighter on the sun-facing side of the canopy and darker on the side of the canopy facing away from the sun (herein referred to as the "crown-shape effect").

Previously proposed topographic normalizations include the cosine, Minnaert, and C corrections [see Fig. 1(a)], as well as sun–canopy–sensor (SCS) approaches [see Fig. 1(b)] [6], [7], [9], [16], [17]. The cosine method is important in using digital elevation models (DEMs) for modeling the illumination of a surface [18]–[20]. This approach assumes that illumination at a particular area is determined by single direction radiance, but it is problematic because of other incoming lights diffused from sky or neighbors. This limitation causes overcorrection on steep surfaces [9], [17]. Also, the use of the same correcting factor for all spectral bands makes it unsuitable for multiband

Manuscript received September 13, 2010; revised November 9, 2011, January 24, 2012, and May 25, 2012; accepted May 26, 2012.

Y. Song and J. Imanishi are with the Graduate School of Global Environment Studies, Kyoto University, Kyoto 606-8501, Japan (e-mail: song.youngkeun.3r@kyoto-u.ac.jp; imanishi@kais.kyoto-u.ac.jp).

H. Hashimoto is with the Department of Environmental Bioscience, Meijo University, Nagoya 468-8502, Japan (e-mail: hihashi@meijo-u.ac.jp).

A. Morimura is with the University of Human Environments, Aichi 444-3505, Japan (e-mail: morimura@uhe.ac.jp).

Y. Morimoto is with the Faculty of Bioenvironmental Science, Kyoto Gakuen University, Kyoto 621-8555, Japan (e-mail: ymo3@me.com).

K. Kitada is with the Nakanihon Air Service Company Ltd., Aichi 480-0202, Japan (e-mail: kkitada@nnk.co.jp).

Color versions of one or more of the figures in this paper are available online at http://ieeexplore.ieee.org.

Digital Object Identifier 10.1109/TGRS.2012.2204404

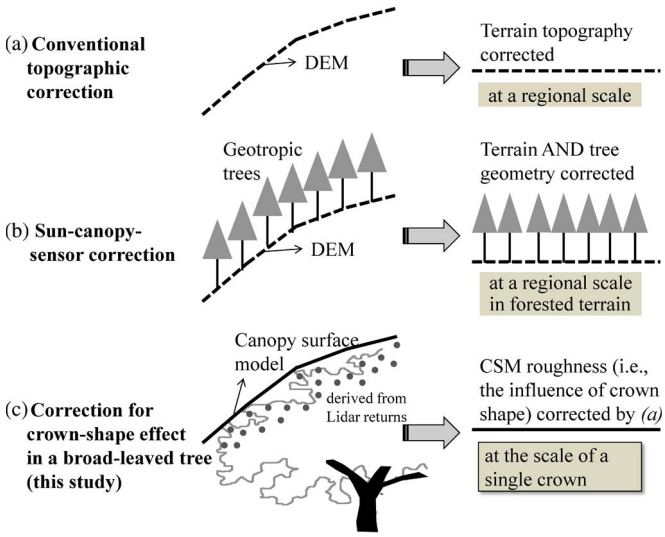

Fig. 1. Conceptual scheme of this study. (a) Conventional topographic normalizations (e.g., cosine, Minnaert, and C corrections). (b) SCS approach. (c) Correction for crown-shape effect at a single-tree level, attempted in the preset study.

imagery [7]. Nevertheless, the cosine correction is the most widely used normalization [7] because of the simple procedure to be followed, without consideration of empirical parameters or dependence of wavelength in the formula (in contrast to the Minnaert and C corrections).

The Minnaert correction [18], [19] is an improvement on the cosine method, employing empirical parameters from the relationship between the modeled and the observed radiance distribution, i.e., taking account of the realistic behavior of surface reflectance. The Minnaert method has been validated by demonstrating a decrease in the variance of the radiance of homogeneous land cover [20] and an increase in the accuracy of forest classification [21]. The C correction [19] also yields enhanced classification performance [9], [10] and improved statistical indicators of the imagery [7], [22]. However, the moderators in these approaches (i.e., the Minnaert constant K and the parameter C) are known to be highly dependent on the type of land cover [20], [22]; therefore, limitations remain when applying these methods to a range of heterogeneous landscapes across a broad area.

The SCS method [16] results in improved topographic corrections for a forest area because it considers both the geometry of the terrain and vertical trees upon the terrain [see Fig. 1(b)]. The approaches that have proved to be useful in correcting forest landscape images [17], [23] also take into account the shadowing effect in canopies [24]. However, the application of such approaches has been limited to coniferous canopies, rather than broad-leaved deciduous trees that are more irregular in shape.

The concept of topographic normalization may also be applied to the correction of crown-shape effect [see Fig. 1(c)]. In such a case, a canopy surface model (CSM) can be used instead of a DEM. In recent years, airborne light detection and ranging (Lidar) remote sensing has enabled CSMs to be acquired in more detail than the scale of a single crown. However, the application of topographic correction to CSM has yet to be studied.

We simply used the term "reflectance" to indicate apparent reflectance, which is obtained from the measured radiance at a particular direction (i.e., scene radiance at the aircraft) after the correction of diffuse sky irradiance (see Section II-D). Therefore, the reflectance may be affected by the geometry among the sun, sensor, and canopy surface. The illumination of canopy surface is dominated by the crown shape of trees, and multi-scattering effects at leaf scale are not considered.

The objective of this study is to correct the influence of crown shape on the spectral reflectance of a single tree. As the methodology, we test the effectiveness of conventional topographic normalizations applied to a CSM, which is derived from airborne small-footprint Lidar data. To evaluate the performances of the correction, we also assess their accuracies in estimating tree vigor (see Section II-B and I), which is an important application of corrected airborne spectral images.

II. Materials and Methods

A. Study Materials and Ground Survey

Spectral corrections were tested on 66 cherry trees (*Cerasus* species) in Yamashina, Kyoto, Japan ($135^\circ\,48'\,54''$ E, $34^\circ\,59'\,41''$ N). The trees are standing on an area of flat terrain bounded by water channels on two sides (see Fig. 2).

The *Cerasus* species is important for the popularity and cultural significance in Japan and is widely planted throughout the country. According to a census in 2003 [25], local authorities in Japan manage 520 491 *Cerasus* trees among a total of 6 785 750 street trees throughout the country. For the large-scale management of these trees, remote sensing studies are required to assess their vigor. At the present study site, cherry trees have been established for several decades as a feature of the local landscape, but some of the trees have recently shown signs of decline.

B. In Situ Assessment of Tree Vigor

In this study, tree vigor is used as an inclusive term that covers the growth and pathological health of a tree, as well as the outer appearance [26]. Therefore, the following diagnostic criteria of tree vigor were employed: foliage, branch, trunk, and pathological concerns [27]. The 66 cherry trees in this study were assessed in terms of the criteria and assigned a grade on a five-point scale (from A = good to E = poor). The tree locations were recorded on an enlarged topographic map (1 : 10 000).

C. Remote Sensing Data

Airborne remote sensing data were acquired simultaneously by spectral imager and Lidar sensors on September 7, 2003, under cloud-free conditions from a flying altitude of 2000 m, at approximately the time of the solar noon given a sun elevation and azimuth of 60° and 195°, respectively. Spectral imagery was obtained using a Compact Airborne Spectrographic Imager (CASI) 1500 (Itres Research Ltd.) with 0.5-m spatial resolution and 12 bands of 10–60 nm full-width at half-maximum (FWHM), covering the visible to near infrared (NIR) region (see Table I). Lidar data, acquired by an Airborne Laser Terrain Mapper 2050 (Optech Inc.), recorded approximately two million returns at 50 kHz, using double-pulse mode and a 38-cm-diameter measurement footprint (see Table I).

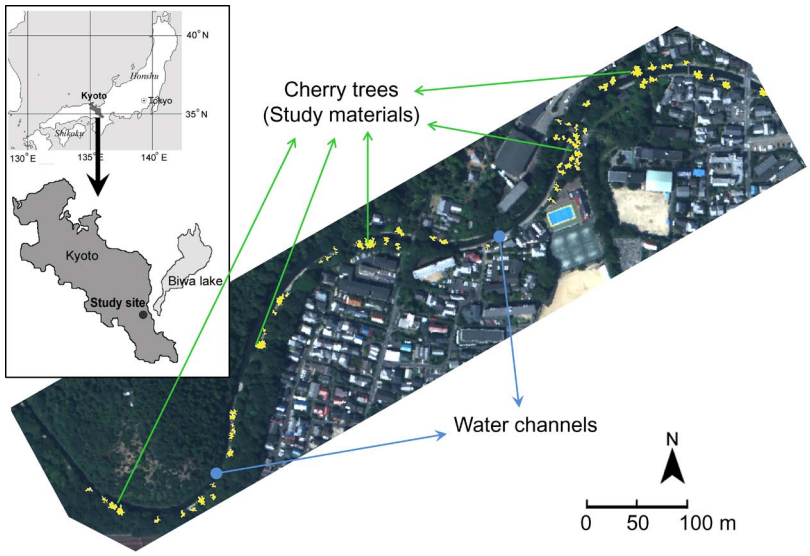

Fig. 2. Location of the study site and study materials. The yellow polygons indicate the crowns of 66 cherry trees selected for this study.

TABLE I
(LEFT-HAND SIDE) BAND DESCRIPTIONS AND SPECTRAL PROPERTIES OF THE CASI SENSOR AND (RIGHT-HAND SIDE) THE SPECIFICATION OF LIDAR MEASUREMENT, EMPLOYED IN THIS STUDY

Band No.	Wavelength (nm)	Band center (nm)	FWHM (nm)	Description
1	397.3–416.9	407.1	9.8	violet
2	415.5–438.1	426.8	11.3	violet
3	436.8–462.4	449.6	12.8	violet–blue
4	461.3–490.1	475.7	14.4	blue
5	489.2–522.4	505.8	16.6	blue–green
6	521.7–560.9	541.3	19.6	green peak
7	560.5–607.7	584.1	23.6	yellow
8	607.6–665.2	636.4	28.8	red
9	665.6–736.0	700.8	35.2	red edge
10	737.1–823.1	780.1	43	near infrared
11	824.9–929.1	877	52.1	near infrared
12	931.8–1057.2	994.5	62.7	near infrared

Sensor	Optech ALTM2050
Scan Angle	0~±20°
Beam Divergence	0.19 mrad
Operating Altitude	2000 m
Footprint diameter	38 cm
Laser repetition rate	50,000 Hz
Scan frequency	20~40 Hz
Flying speed	130 knots
Laser Wavelength	1064 nm
The density of laser pulses	1.3 returns/m^2

D. Atmospheric Correction

In situ spectral data for atmospheric correction were collected by an SE590 spectroradiometer (Spectron Engineering Inc.) at the same time that the aircraft passed overhead. We measured the reflectance on spots of water and asphalt, as well as on a 3 × 3 m white canvas and a $BaSO_4$ panel laid flat upon an open area.

We used the well-known empirical line calibration method [28] which forced the raw CASI digital records to match with *in situ* spectral reflectance. Both the white (canvas and $BaSO_4$ panel) and black (water and asphalt) reference points were adopted and regressed linearly along with each of the 12 bands. Based on the regression results, CASI radiance was converted to a surface reflectance value. This processing was expected to reduce atmospheric and instrumental effects.

E. Preparation of the Canopy Area

To identify the spatial extent of individual tree canopies, ground surveys were performed several times to ensure that the canopy polygons of all the trees were drawn as carefully as possible. For the reference of drawing each crown boundary, we used the enlarged false-color CASI image. The polygons were projected onto remote sensing imagery using the Area Of Interest tool (AOI, ERDAS IMAGINE 8.7). All of the AOIs were drawn on the most probable canopy area of each individual tree, without mutual overlap [see Fig. 3(a)].

F. Derivation of the CSM

The procedure for correction involves deriving an appropriate CSM from Lidar data and applying conventional topographic normalizations to the CSM instead of to a DEM. Before producing the CSM, the point clouds of Lidar data were filtered (i.e., data thinning) because many of the returns are reflected from below the canopy surface [29]. The returns cause pits in the CSM because of their much lower altitude compared with neighboring points [30], in the case that all of the returns are employed in triangulated irregular network (TIN) surface modeling. Although the pits may exist in reality, they do not

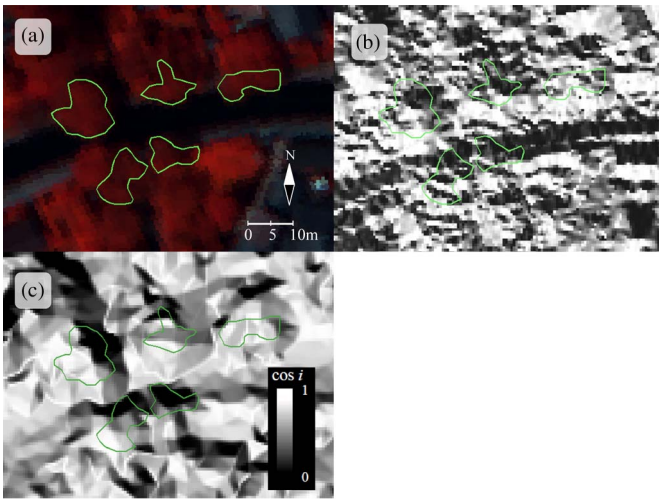

Fig. 3. Example of visual assessment. (a) False-color image employing CASI bands 11 (as red), 6 (as green), and 4 (as blue). Illumination figures (i.e., cosine of incidence angle) of the CSMs canopy surface models derived from (b) unfiltered Lidar point-cloud dataset, and (c) filtered with $A = 0.5$ and $B = 1.5$. The green-boundary polygons exhibit the canopy area of trees.

represent the elevation of the adjacent canopies and therefore contribute little to depicting the overall appearance of the crown shape. Thus, we eliminated the below-CSM returns by using "thin point processing" in Terrascan software [31], employing the following steps: 1) Keep the point of highest elevation within every horizontal distance of A m, and 2) take the average elevation value of the points within every horizontal distance of B m. These steps were adopted to do the following: 1) to remove the influence of lows within a given pixel size (A m) and 2) to smoothen the influence of remaining local lows at the scale of an individual tree canopy (B m). We generated several CSMs using TIN. The values of A and B were systemically tested from 0.5 to 3.0, at 0.5-m intervals, considering the spatial resolution of the CASI imagery (0.5 m) and the size of the crown. From all of the tested surfaces, we calculated the illumination figures for every case, in terms of (2.1) (see Section II-G). The surfaces were visually assessed to ensure that any pits were filled in the figure and that the geometry of upper tree crowns was well represented [e.g., Fig. 3(b) and (c)].

We selected the surface with $A = 0.5$ and $B = 1.5$ as the best case [see Fig. 3(c)]. Consequently, the spatial scale of the CSM becomes dependent on the sizes of the triangles generated from the filtered dataset. The CSM was resampled to match the spatial resolution of CASI image.

G. Application of Topographic Normalizations to the CSM

According to the concept upon which this study is based (see Fig. 1), the SCS model is applicable to groups of trees standing on the landscape, and the present study concerns individual canopies only. In other words, if the SCS terrain is regarded as the CSM in this study, geotropic trees on the SCS terrain would presumably have no corresponding material standing on the CSM. Therefore, we tested three conventional topographic normalizations, except for the SCS method, in terms of the CSM of single crowns: the cosine, Minnaert, and C corrections.

The cosine correction assumes that the amount of irradiance reaching a pixel on a slope is directly proportional to the cosine of the incidence angle ($\cos i$), where the incidence i denotes the angle between the surface normal and the solar beam, which can be calculated as follows [7], [12], [18]–[20], [32], [33]:

$$\cos i = \cos\theta_p \cdot \cos\theta_z + \sin\theta_p \cdot \sin\theta_z \cdot \cos(\phi_a - \phi_o) \quad (2.1)$$

where θ_p is the slope angle, θ_z is the solar zenith angle, ϕ_a is the solar azimuth angle, and ϕ_o is the slope orientation (i.e., aspect) angle.

The nonverticality of sun rays onto an inclined pixel is corrected in terms of simple trigonometry, i.e., the reflectance value is compensated by the incidence angle i and diminished by the solar zenith angle θ_z

$$L_H = L_T \cdot \left(\frac{\cos\theta_z}{\cos i}\right) \quad (2.2)$$

where L_H is the reflectance of a horizontal surface and L_T is the reflectance of an inclined surface.

However, the reflectance in reality is not always proportional to $\cos i$ because of the effect of indirect (i.e., diffuse) irradiance, particularly in cases where i is large [19].

The Minnaert approach introduced the parameter K_n of each n band to (2.2), as a measure of the extent to which a surface follows the Lambertian assumption of cosine correction

$$L_H = L_T \cdot \left(\frac{\cos\theta_z}{\cos i}\right)^{Kn} \quad (2.3)$$

where K_n is the Minnaert constant for band n.

The parameter K_n can be empirically obtained from the slope of the linearized (2.3) after logarithmic transformation [7], [9]. The value of K_n varies between 0 and 1; high values of K_n indicate that the reflectance at band n is corrected by closer computation to the Lambertian assumption of the cosine method, whereas lower values mean that band n is less influenced by inclination to the sun (i.e., the incidence angle).

In the C correction, the parameter C_n of each band n moderates the cosine correction (2.2) (as does K_n in Minnaert)

$$L_T = m \cdot cos\ i + b \quad (2.4)$$

where m is the slope of the regression line, b is the intercept of the regression line, and

$$L_H = L_T \cdot \left(\frac{\cos\theta_z + C_n}{\cos i + C_n}\right) \quad (2.5)$$

where C_n is the constant for band n; $C_n = b_n/m_n$.

The results obtained for the three methods were compared in terms of the correlation between reflectance and $\cos i$. An ideal correction would lead to a correlation coefficient r of zero, which would indicate that the reflectance is irrelevant to the incident angles, in turn meaning that the topographic effect (i.e., the crown-shape effect in the present case) has been normalized [10], [22], [32], [33].

TABLE II
ASSESSMENT OF ACCURACY IN CASES (LOWER) *WITH* AND (UPPER) *WITHOUT* CORRECTION. VALUES ARE THE MEANS OF DISCRIMINANT ANALYSES ITERATED TEN TIMES. CONVENTIONAL LOGIC ACCEPTS ONLY (DARK GRAY) DIAGONAL CELLS, WHEREAS FUZZY LOGIC ALSO ACCEPTS (LIGHT GRAY) ADJACENT CELLS. THE DIFFERENCES BETWEEN (UPPER) UNCORRECTED AND (LOWER) C-CORRECTED ASSESSMENTS ARE SHOWN IN PARENTHESES. ABBREVIATIONS: PA = PRODUCER'S ACCURACY, FPA = FUZZY PRODUCER'S ACCURACY, UA = USER'S ACCURACY, AND FUA = FUZZY USER'S ACCURACY

		Ground Reference Data							
	Rank	A	B	C	D	E	Row Total	UA(%)	FUA(%)
Remote Sensing Data	A	**6.3**	2.1	2.8	1.2	0.0	**12.4**	50.8	67.7
	B	2.8	**1.5**	2.5	1.6	0.0	**8.4**	17.9	81.0
	C	0.1	1.0	**1.7**	2.8	0.1	**5.7**	29.8	96.5
	D	0.2	1.0	3.3	**2.9**	0.5	**7.9**	36.7	84.8
	E	0.6	0.9	2.3	4.4	**1.4**	**9.6**	14.6	60.4
	Column Total	**10.0**	**6.5**	**12.6**	**12.9**	**2.0**	**44.0**		
	PA (%)	63.0	23.1	13.5	22.5	70.0			
	FPA (%)	91.0	70.8	59.5	78.3	95.0			
Overall accuracy (%)		31.4							
Overall fuzzy accuracy (%)		**75.5**							

Uncorrected assessment

		Ground Reference Data							
	Rank	A	B	C	D	E	Row Total	UA(%)	FUA(%)
Remote Sensing Data	A	**6.6** *(+0.3)*	1.6 *(-0.5)*	2.1 *(-0.7)*	1.0 *(-0.2)*	0.0 *(-)*	**11.3** *(-1.1)*	58.4 *(+7.6)*	72.6 *(+4.9)*
	B	3.4 *(+0.6)*	**1.4** *(-0.1)*	2.8 *(+0.3)*	1.5 *(-0.1)*	0.0 *(-)*	**9.1** *(+0.7)*	15.4 *(-2.5)*	83.5 *(+2.5)*
	C	0.0 *(-0.1)*	2.4 *(+1.4)*	**4.2** *(+2.5)*	3.1 *(+0.3)*	0.0 *(-0.1)*	**9.7** *(+4.0)*	43.3 *(+13.5)*	100.0 *(+3.5)*
	D	0.0 *(-0.2)*	0.5 *(-0.5)*	2.4 *(-0.9)*	**1.9** *(-1.0)*	0.2 *(-0.3)*	**5.0** *(-2.9)*	38.0 *(+1.3)*	90.0 *(+5.2)*
	E	0.0 *(-0.6)*	0.6 *(-0.3)*	1.1 *(-1.2)*	5.4 *(+1.0)*	**1.8** *(+0.4)*	**8.9** *(-0.7)*	20.2 *(+5.6)*	80.9 *(+20.5)*
	Column Total	**10.0** *(-)*	**6.5** *(-)*	**12.6** *(-)*	**12.9** *(-)*	**2.0** *(-)*	**44.0** *(-)*		
	PA (%)	66.0 *(+3.0)*	21.5 *(-1.6)*	33.3 *(+19.8)*	14.7 *(-7.8)*	90.0 *(+20.0)*			
	FPA (%)	100.0 *(+9.0)*	83.1 *(+12.3)*	74.6 *(+15.1)*	80.6 *(+2.3)*	100.0 *(+5.0)*			
Overall accuracy (%)		36.1 *(+4.7)*							
Overall fuzzy accuracy (%)		**84.5** ***(+9.0)***							

C corrected assessment

H. NDVI Mask

A normalized difference vegetation index (NDVI) [34] mask was introduced to exclude non-vegetation pixels in canopy polygons. These polygons are likely to include some background pixels of water, soil, or asphalt. NDVI, which is widely accepted as a means of discriminating between areas of vegetation and nonvegetation, was used in the scaling procedure with a threshold value of 0.5 [35]. It masked out 239 non-vegetation pixels from 10 285 tree pixels, thereby producing AOIs with more homogeneous canopies. Note that the corrections outlined in Section II-G were more applicable to the spectra of homogeneous targets (see Section I). From the preprocessed imagery, we finally prepared the spectral information inventory of all the target trees by recording the mean spectral values within each AOI.

I. Discriminant Analysis and Assessment of Accuracy

The ratio of red edge (band 9) to green (band 6), related to the chlorophyll content at the canopy scale, was selected as the best vegetation index because it yielded the highest correlation with *in situ* tree vigor (Spearman's $r_s = 0.659$, $p < 0.01$, $n = 66$) among all the tested indices and other potential spectral combinations, yielding a higher correlation than the NDVI ($r_s = 0.347$) [27]. Using this index, we developed discriminant models ($p < 0.05$) from a stratified random sample of one-third of the trees ($n = 22$) and used the models to grade the remaining two-thirds ($n = 44$) into one of the five ranks (A: good; E: poor).

The classes of tree vigor defined in this study are not mutually exclusive: They grade into each other, as described in previous applications to a vegetated area [36], [37]. In accuracy assessment, these previous studies enlarged the diagonal classes of the error matrix into adjacent grades (i.e., fuzzification) as a "support" category for the correct determination. Employing fuzzy logic, we permitted "correct" and "acceptable" classifications [38], [39].

A discriminant model may induce anomalous results unless the random sample for the model is large enough to include the features of all the vigor groups. To avoid such anomalous results, we iterated the preceding classifying procedure ten times and recorded the mean values (see Table II).

J. Validation of Correction Procedures

All the data processing was separately conducted for both *with* and *without* spectral correction of trees (see Fig. 4). The statistical significance of the differences between the two approaches was assessed by an independent t-test, and the overall fuzzy accuracies were obtained from ten repetitions of assessments of tree vigor (see Section II-I). Table II shows a detailed comparison of the two approaches.

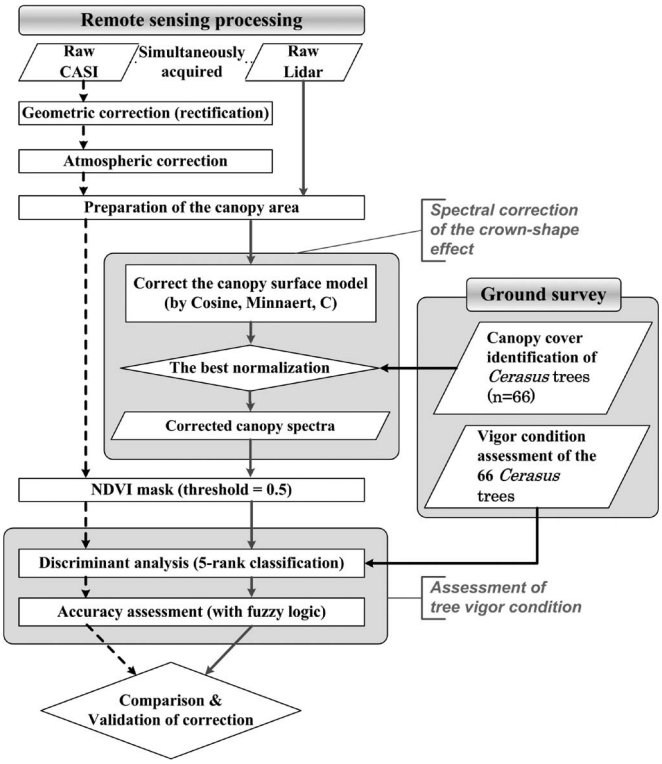

Fig. 4. Flow diagram of the study designed to assess differences between (gray solid lines) *with* and (black dashed lines) *without* spectral correction of the crown-shape effect.

K. Assumptions

This study assumed that the differences in spectral features of trees were mainly dependent on the geometry of crown shape and on the vigor condition. This assumption was made because the trees are of the same genus, suggesting little effect from inherent differences in leaf and canopy morphologies, and because the trees are standing on flat terrain, which means that the roughness of the canopy surface is the only geometric factor that affects canopy reflectance. Moreover, for simplification, we assumed that the spectral reflectance for each tree is derived from the upper layer of the crown. This assumption was made because the upper crowns are relatively dense and continuous, meaning that they would be dominated by the geometry of the canopy surface, with little effect from shadows among branches or leaves at a smaller spatial scale. In addition, the procedure followed in preparing the study area (see Section II-E) was intended to avoid the effect from neighboring trees (e.g., mutual shadowing) as much as possible, meaning that such effects could be ignored in each AOI.

III. Results

A. Evaluation of Correction Methods

The correlation coefficient r in Table III indicates the effect of the incident angle on canopy reflectance. The C correction was the best method in terms of yielding coefficients close to zero in all bands, indicating the greatest reduction in the influence of crown shape on the tree spectrum. The performance of the C correction is shown in Fig. 5.

TABLE III
PARAMETERS AND CORRELATION COEFFICIENTS IN ASSESSING THE PERFORMANCE OF THREE CORRECTION METHODS. FOR EACH BAND, WE DERIVED THE INCLINATION m, THE INTERCEPT b, THE CONSTANT C FOR C CORRECTION, AND K FOR MINNAERT. CORRELATION COEFFICIENTS WERE OBTAINED FROM THE REGRESSION LINE BETWEEN REFLECTANCE AND INCIDENCE ANGLE. THE CORRELATION r BECAME CLOSE TO ZERO FOR CORRECTED DATA

Band No.	Parameters				Correlation coefficient r			
	m	b	C	K	Uncorrecte	Cosine	Minnaert	C
1	0.0108	0.0278	2.5869	0.1039	0.1853	-0.0295	0.0160	0.0003
2	0.0081	0.0276	3.4076	0.0662	0.1805	-0.0257	0.0394	0.0015
3	0.0068	0.0299	4.4164	0.0518	0.1629	-0.0264	0.0364	0.0018
4	0.0069	0.0271	3.9491	0.0571	0.1647	-0.0253	0.0408	0.0012
5	0.0076	0.0275	3.6003	0.0679	0.1707	-0.0244	0.0387	0.0012
6	0.0138	0.0407	2.9572	0.0869	0.2319	-0.0255	0.0387	0.0024
7	0.0133	0.0347	2.6081	0.0975	0.2088	-0.0253	0.0383	0.0010
8	0.0111	0.0272	2.4411	0.0975	0.1807	-0.0252	0.0458	-0.0007
9	0.0208	0.0592	2.8492	0.0867	0.2404	-0.0274	0.0522	0.0005
10	0.0723	0.2398	3.3171	0.0753	0.2512	-0.0282	0.0460	0.0026
11	0.0824	0.2892	3.5089	0.0695	0.2466	-0.0285	0.0495	0.0025
12	0.0852	0.3241	3.8024	0.0632	0.2427	-0.0286	0.0526	0.0022

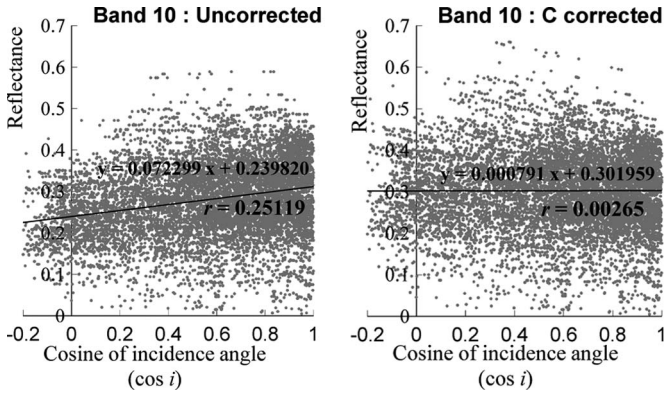

Fig. 5. Relationship between reflectance and cosine of the incidence angle $(\cos i)$ of band 10.

In Table III, negative values of r for cosine correction indicate overcorrection, as also reported in previous studies [9], [17]; this occurs when the incidence angle approaches 90° (i.e., $\cos i$ is close to 0). The occurrence of pixels with smaller values of $\cos i$ results in smaller values of the denominator in (2.2), in turn resulting in extremely brighter or saturated pixel values than expected (i.e., overcorrection). The failure of correction indicated in previous studies [9], [17] based on DEMs is also apparent in the application to a CSM in the present study.

Only the C correction was applicable to pixels with $\cos i$ values less than 0 (i.e., steep surfaces with an incidence angle exceeding 90°) because these pixels were computable only by (2.5). However, in the Minnaert correction, a negative value of $\cos i$ causes a calculation error because $0 \leq K_n \leq 1$ [7], [9], [17] and because the base $\cos \theta_z / \cos i$ should be positive, where θ_z was constant at 30° in this study (2.3). Consequently, the 608 pixels with subzero $\cos i$ values (data not shown) could not be calculated by the Minnaert correction. The cosine method also converted the subzero $\cos i$ pixels to negative values according to (2.2), which yielded nonexistent reflectance values.

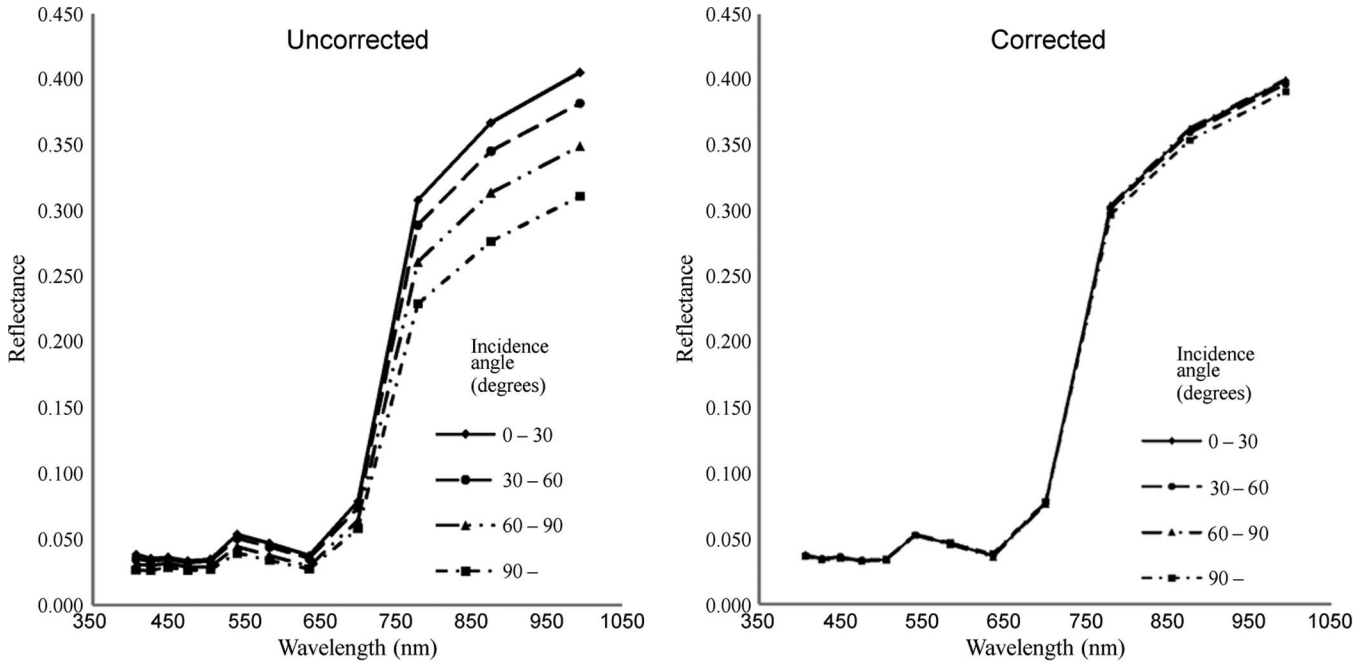

Fig. 6. Change in tree spectra following C correction, considering the incidence angle of the canopy surface. All the pixels were grouped and averaged in terms of a given range of incidence angle. The number of pixels in each group was as follows: 2219 pixels for 0°–30° (21.6%), 4336 pixels for 30°–60° (42.2%), 3122 pixels for 60°–90° (30.3%), and 608 pixels for over 90° (5.9%). The mean spectra of each group are shown (left) *with* and (right) *without* correction.

B. Change in Spectral Characteristics After Correction

Fig. 6 summarizes the effect of correction on the study pixels. Uncorrected spectra showed variations in terms of incidence angle. Reflectance from a surface with a higher incidence angle (i.e., a more steeply inclined portion) tended to less-illuminated values for all bands (see the left-hand side of Fig. 6). However, this variation was greatly reduced by the correction procedures (see the right-hand side of Fig. 6). The less-illuminated values of steeply inclined surfaces were compensated to values close to those for the reflectance of a horizontal surface.

C. Comparison of Performance Between With and Without Spectral Correction of Trees

The overall fuzzy accuracy in assessing tree vigor condition was significantly increased *with* spectral correction (see Table II), in estimations based on ten iterations ($p < 0.001$, two-tailed, independent t-test). The overall accuracy, using fuzzy logic, was improved from 75.5% to 84.5% with the spectral correction, and the accuracy of rank assessments was also increased (numbers in parentheses in Table II), particularly for ranks C and E. The data in the table regarding the estimated number of trees reveal that correct or acceptable results generally increased (dark or light gray cells, respectively. See Section II-I), whereas unacceptable assessments decreased (uncolored cells).

An example of a notable enhancement in accuracy was found for ground-based rank C trees (see Table II). *Without* correction (upper block in the table), a mean number of 2.3 trees of ground-rank C were incorrectly assigned a rank of E based on remote sensing data. *With* correction (lower block), a mean number of 1.2 trees turned to be correctly assigned among the incorrect results by remote sensing, and the accuracies were improved: The increases in the producer's accuracy of ranks C and E were 19.8% and 20.0%, respectively, and the increases in the fuzzy producer's accuracy of ranks C and E were 15.1% and 5.0%, respectively. For users who would employ this remote assessment, it is important that the correction yielded greater accuracies for estimating rank C (i.e., user's accuracy increased by 13.5% and fuzzy user's accuracy achieved 100%) and rank E (i.e., fuzzy user's accuracy increased by 20.5%). Similar improvements following correction were found for some trees with ground ranks of B and A.

IV. Discussion

A. Correction for Steeply Inclined Surfaces

A portion of the CSM was inclined with an incidence angle greater than 90°. Such an angle has not been considered in previous studies, although surfaces approaching an incidence angle of 90° have been mentioned [9], [17], [19]. The spectra of steeply inclined (and consequently shaded) surfaces are strongly influenced by diffuse irradiance, meaning that cosine correction based on a Lambertian assumption is inappropriate. However, in the case of a surface with an incidence angle greater than 90°, only the C correction (among the methods tested in the present study) was mathematically applicable for correcting the diffuse irradiance effect on the canopy. We believe that these steep surfaces ($> 90°$) arose because of differences in the resolutions of the DEM and CSM used for the illumination modeling. The small-footprint Lidar data employed in the present study provided the CSM with a sufficiently high spatial resolution to depict the rough parts of the canopy, to the extent of dozens of pixels in describing the surface of a single crown. On the other hand, previous studies [7]–[12], [20]–[22] employed a DEM with a spatial resolution greater than 25 m

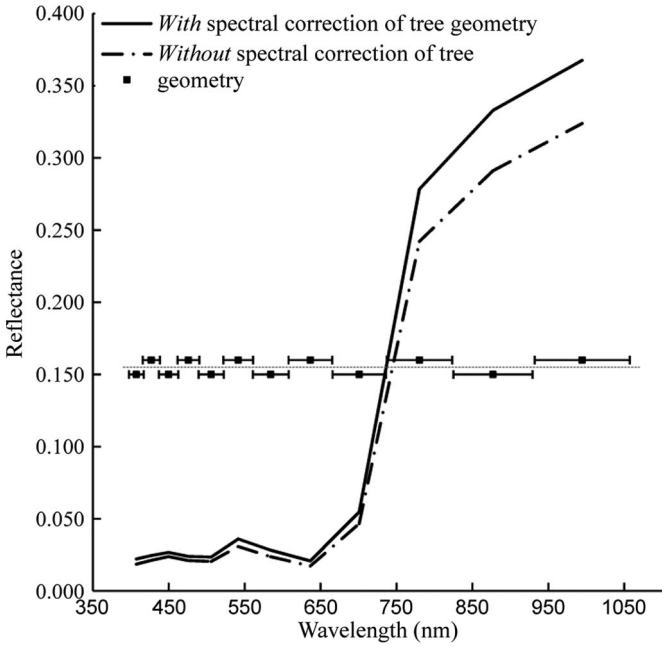

Fig. 7. Example of a reflectance spectrum (for tree ID 14_00). Following topographic correction by the C method, the reflectance spectrum was changed from that shown by the dot-dashed line to that shown by the solid line. The dots and bars indicate the center wavelength and half bandwidth of each band employed in this study (see Table I).

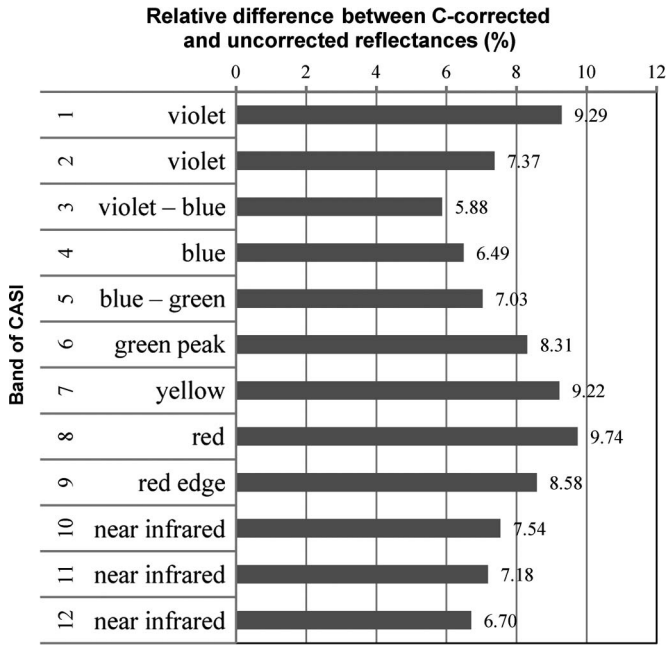

Fig. 8. Change in the reflectance of each band following C correction. The difference between *with* and *without* correction was evaluated for each band, from mean pixel values for the entire study area. Numbers on bars indicate the percent ratio of the difference to *without*-correction reflectance.

and Landsat TM images. It appears that the spatial resolution and scale of study were larger in the previous studies than in the present study, meaning that inclined portions with an incidence angle $> 90^\circ$ were rarely found.

B. Effect of Correction on Spectral Reflectance of a Single Tree

In the present study, spectral correction was successful in compensating the reduced radiance from the inclined portions of a canopy surface (see Fig. 6). Fig. 7 shows that the correction had an effect on the result of vigor assessment, which was conducted with the remotely sensed tree spectrum. The tree shown in Fig. 7 was incorrectly assigned a rank of E in the case of *without* correction (dot-dashed line); a rank of A was assigned on the ground. However, *with* correction (solid line in Fig. 7), the corrected spectrum improved the result of vigor assessment to a rank of B, which became closer to the on-ground result (A) and was an "acceptable" result in terms of fuzzy accuracy (meaning that the tree would be included in the light gray cells in the lower block of Table II).

Fig. 7 also shows that the improvement was associated with an increase in the reflectance of all bands. In terms of absolute difference, i.e., simply taking the difference between *with*-correction reflectance (solid line) and *without*-correction reflectance (dot-dashed line), the reflectance was greatly increased at the NIR region. This type of critical change in NIR has also been shown to be typical of the difference in the radiance between sunlit and shadow areas [40], [41]. This type of feature at the NIR region has been used to minimize the decrease in canopy reflectance in terms of shadowing, by selecting only canopy pixels with high NIR reflectance [42], [43]. Moreover, NIR reflectance is often used as a key factor in the remote sensing of vegetation (e.g., in vegetation indices); hence, the crown-shape effect on a tree spectrum should be carefully considered in future studies.

The crown-shape effect varied with wavelength (see Fig. 8). In terms of the relative difference (ratio) between *with* and *without* correction, the red region was the most strongly affected (9.74%), followed by the red edge (8.58%) and green peak (8.31%); NIR (7.54%) showed the largest absolute difference. In previous studies, operations among bands (e.g., the band ratio) were expected to offset a probable slope and aspect effect at a terrain scale, under the assumption that the reflectance of bands would be proportional to the magnitude of the effect (refer to the reviews in [7] and [20]). However, at the scale of a single crown, variations in the crown-shape effect among different bands indicate that further consideration of band operations is needed in subsequent spectral analyses.

The tree spectra of the *without*-correction may contain less-illuminated pixels in inclined portions of crowns (see Figs. 6 and 7). These pixels act to degrade the spectra (e.g., the dot-dashed line in Fig. 7), resulting in an incorrect estimation. Following correction, the spectra were compensated, particularly in trees with a ground rank of E or D, resulting in improved accuracies (see the lower block in Table II).

C. Application to Other Tree Species

The correction method proposed in this study can be applied to the closed canopy of broad-leaved tree species. Note that our experiments were carried out based on the assumptions in Section II-K. The assumptions do not directly limit tree species but limit the figure of dense and continuous upper crowns and the no mutual-shadowing effect from adjacent trees. This situation is often found in a cluster of broad-leaved trees at the similar developing stages. On the other hand, many cases of coniferous standing or hierarchical canopy structure may be far

from the situation of our assumption. If the shadows among trees and gaps in the canopy are apparent in the image, the illumination of canopy surface cannot be modeled only by the geometry of Lidar-derived CSM.

V. Conclusion

The shape of the tree crown has a strong influence on the canopy reflectance of a single tree, as observed in remote sensing imagery. For the correction processing (i.e., normalization), it was useful to assume that the roughness of the canopy surface within a single crown resembles the topography of the land surface. This approach was appropriate in the case of a closed canopy of broad-leaved deciduous trees because the illumination of dense and continuous upper crowns could be modeled based on the CSM derived from small-footprint Lidar data. The C-correction method proved to be the most successful in the normalization of the CSM. This method was particularly effective in correcting the less-illuminated pixels of canopy surfaces with an incidence angle $> 90^\circ$, for which the cosine and Minnaert methods generated calculation errors. The crown-shape effect was greater at the NIR region in terms of absolute difference between the spectra *with* and *without* correction and at the red region in terms of relative difference. Because the effect varied with wavelength, it could not be fully corrected by conventional band-ratio operations.

The correction of tree spectra resulted in an improvement of overall fuzzy accuracy from 75.5% to 84.5%, when assessing the vigor condition using the spectra. This result indicates that the crown-shape effect should be carefully considered in single-crown-level analyses of remote sensing data.

Future studies should address the following issues: estimating the geometry of tree-crown shape in areas of rugged terrain, developing quantitative criteria for selecting an appropriate CSM, and assessing the difference between CSM and DEM applications in terms of the effect of rugged surface on spectral reflectance.

References

[1] X. Li and A. H. Strahler, "Geometric-optical bidirectional reflectance modeling of the discrete crown vegetation canopy: Effect of crown shape and mutual shadowing," *IEEE Trans. Geosci. Remote Sens.*, vol. 30, no. 2, pp. 276–292, Mar. 1992.

[2] X. Li and A. H. Strahler, "Geometric-optical modeling of a conifer forest canopy," *IEEE Trans. Geosci. Remote Sens.*, vol. GE-23, no. 5, pp. 705–721, Sep. 1985.

[3] X. Li and A. H. Strahler, "Geometric-optical bidirectional reflectance modeling of a conifer forest canopy," *IEEE Trans. Geosci. Remote Sens.*, vol. GE-24, no. 6, pp. 906–919, Nov. 1986.

[4] A. H. Strahler and C. E. Woodcock, "A hybrid geometric optical-radiative transfer approach for modeling albedo and directional reflectance of discontinuous canopies," *IEEE Trans. Geosci. Remote Sens.*, vol. 33, no. 2, pp. 466–480, Mar. 1995.

[5] J. Franklin and D. L. Turner, "The application of a geometric optical canopy reflectance model to semiarid shrub vegetation," *IEEE Trans. Geosci. Remote Sens.*, vol. 30, no. 2, pp. 293–301, Mar. 1992.

[6] D. Gu, A. R. Gillespie, J. B. Adams, and R. Weeks, "A statistical approach for topographic correction of satellite images by using spatial context information," *IEEE Trans. Geosci. Remote Sens.*, vol. 37, no. 1, pp. 236–246, Jan. 1999.

[7] D. Riano, E. Chuvieco, J. Salas, and I. Aguado, "Assessment of different topographic corrections in Landsat-TM data for mapping vegetation types," *IEEE Trans. Geosci. Remote Sens.*, vol. 41, no. 5, pp. 1056–1061, May 2003.

[8] C. Conese, M. A. Gilabert, F. Maselli, and L. Bottai, "Topographic normalization of TM scenes through the use of an atmospheric correction method and digital terrain models," *Photogramm. Eng. Remote Sens.*, vol. 59, no. 12, pp. 1745–1753, 1993.

[9] P. Meyer, K. I. Itten, T. Kellenbenberger, S. Sandmeier, and R. Sandmeier, "Radiometric corrections of topographically induced effects on Landsat TM data in an alpine environment," *ISPRS J. Photogramm. Remote Sens.*, vol. 48, no. 4, pp. 17–28, 1993.

[10] K. I. Itten and P. Meyer, "Geometric and radiometric correction of TM data of mountainous forested areas," *IEEE Trans. Geosci. Remote Sens.*, vol. 31, no. 4, pp. 764–770, Jul. 1993.

[11] H. Huang, P. Gong, N. Clinton, and F. Hui, "Reduction of atmospheric and topographic effect on Landsat TM data for forest classification," *Int. J. Remote Sens.*, vol. 29, no. 19/20, pp. 5623–5642, Oct. 2008.

[12] S. Ekstrand, "Landsat TM-based forest damage assessment: Correction for topographic effects," *Photogramm. Eng. Remote Sens.*, vol. 62, no. 2, pp. 151–161, 1996.

[13] R. L. Johnson, D. R. Peddle, and R. J. Hall, "A modeled-based sub-pixel scale mountain terrain normalization algorithm for improved LAI estimation from airborne CASI imagery," in *Proc. 22nd Can. Symp. Remote Sens.*, Victoria, BC, Canada, Aug. 21–25, 2000, pp. 415–424.

[14] P. Birnbaum, "Canopy surface topography in a French Guiana forest and the folded forest theory," *Plant Ecol.*, vol. 153, no. 1/2, pp. 293–300, 2001.

[15] D. S. Culvenor, "Extracting individual tree information," in *Remote Sensing of Forest Environments*, M. A. Wulder and S. E. Franklin, Eds. Norwell, MA: Kluwer, 2003, ch. 9, pp. 258–262.

[16] D. Gu and A. R. Gillespie, "Topographic normalization of Landsat TM images of forest based on subpixel sun–canopy–sensor geometry," *Remote Sens. Environ.*, vol. 64, no. 2, pp. 166–175, May 1998.

[17] S. A. Soenen, D. R. Peddle, and C. A. Coburn, "SCS+C: A modified sun-canopy-sensor topographic correction in forested terrain," *IEEE Trans. Geosci. Remote Sens.*, vol. 43, no. 9, pp. 2148–2159, Sep. 2005.

[18] J. A. Smith, T. L. Lin, and K. J. Ranson, "The Lambertian assumption and Landsat data," *Photogramm. Eng. Remote Sens.*, vol. 46, no. 9, pp. 1183–1189, 1980.

[19] P. M. Teillet, B. Guindon, and D. G. Goodenough, "On the slope-aspect correction of multispectral scanner data," *Can. J. Remote Sens.*, vol. 8, no. 2, pp. 84–106, 1982.

[20] J. D. Colby, "Topographic normalization in rugged terrain," *Photogramm. Eng. Remote Sens.*, vol. 57, no. 5, pp. 531–537, May 1991.

[21] T. Tokola, J. Sarkeala, and M. V. D. Linden, "Use of topographic correction in Landsat TM-based forest interpretation in Nepal," *Int. J. Remote Sens.*, vol. 22, no. 4, pp. 551–563, 2001.

[22] E. R. McDonald, X. Wu, P. Caccetta, and N. Campbell, Illumination correction of Landsat TM data in South East NSW, Environment Australia, Canberra, Australia. [Online]. Available: http://www.environment.gov.au/land/publications/illumination.html

[23] S. A. Soenen, D. R. Peddle, C. A. Coburn, R. J. Hall, and F. G. Hall, "Improved topographic correction of forest image data using a 3-D canopy reflectance model in multiple forward mode," *Int. J. Remote Sens.*, vol. 29, no. 4, pp. 1007–1027, Feb. 2008.

[24] V. Kane, A. Gillespie, R. Mcgaughey, J. Lutz, K. Ceder, and J. Franklin, "Interpretation and topographic compensation of conifer canopy self-shadowing," *Remote Sens. Environ.*, vol. 112, no. 10, pp. 3820–3832, Oct. 2008.

[25] "The Street Tree of Our Country V," N.I.L.I.M., Tsukuba City, Japan, Tech. Note N.I.L.I.M. 149, p. 31, Mar. 2004.

[26] M. Ferretti, "Forest health assessment and monitoring—Issues for consideration," *Environ. Monit. Assess.*, vol. 48, no. 1, pp. 45–72, Oct. 1997.

[27] Y. K. Song, J. Imanishi, H. Hashimoto, A. Morimura, and Y. Morimoto, "Importance of the green spectral region for remote assessment of tree vigor condition: A case study of Cerasus species," *J. Environ. Inf. Sci.*, vol. 39, no. 5, pp. 87–96, Mar. 2011.

[28] J. R. Jensen, *Introductory Image Processing: A Remote Sensing Perspective*, 3rd ed. Upper Saddle River, NJ: Prentice-Hall, 2004, ch. 6, pp. 210–213.

[29] S. Solberg, E. Næsset, and O. M. Bollandsås, "Single tree segmentation using airborne laser scanner data in a heterogeneous spruce forest," *Photogram. Eng. Remote Sens.*, vol. 72, no. 12, pp. 1369–1378, Dec. 2006.

[30] J. R. Ben-Arie, G. J. Hay, R. P. Powers, G. Castilla, and B. St-Onge, "Development of a pit filling algorithm for LiDAR canopy height models," *Comput. Geosci.*, vol. 35, no. 9, pp. 1940–1949, Sep. 2009.

[31] *TerraScan User's Guide*, Terrasolid Ltd., 2010.

[32] D. L. Civco, "Topographic normalization of Landsat Thematic Mapper digital imagery," *Photogramm. Eng. Remote Sens.*, vol. 55, no. 9, pp. 1303–1309, Sep. 1989.

[33] S. Kobayashi and K. Sanga-Ngoie, "The integrated radiometric correction of optical remote sensing imageries," *Int. J. Remote Sens.*, vol. 29, no. 19/20, pp. 5957–5985, Oct. 2008.
[34] J. W. Rouse, R. H. Haas, J. A. Schell, D. W. Deering, and J. C. Harlan, "Monitoring the Vernal advancements and retrogradation (Greenwave effect) of nature vegetation," NASA, Washington, DC, p. 371, 1974, NASA/GSFC Final Rep..
[35] Q. Xiao, S. L. Ustin, and E. G. McPherson, "Using AVIRIS data and multiple-masking techniques to map urban forest tree species," *Int. J. Remote Sens.*, vol. 25, no. 24, pp. 5637–5654, Dec. 2004.
[36] J. R. Jensen, *Introductory Image Processing: A Remote Sensing Perspective*, 3rd ed. Upper Saddle River, NJ: Prentice-Hall, 2004, ch. 13, pp. 508–512.
[37] R. G. Congalton and K. Green, *Assessing the Accuracy of Remotely Sensed Data: Principles and Practices*, 2nd ed. Boca Raton, FL: CRC Press, 2008, ch. 9, pp. 131–140.
[38] L. C. Raymond, "Accuracy assessment of maps of forest condition: Statistical design and methodological considerations," in *Remote Sensing of Forest Environments*, M. A. Wulder and S. E. Franklin, Eds. Norwell, MA: Kluwer, 2003, ch. 5, pp. 115–140.
[39] C. Woodcock and S. Gopal, "Fuzzy set theory and thematic maps: Accuracy assessment and area estimation," *Int. J. Geogr. Inf. Sci.*, vol. 14, no. 2, pp. 153–172, Mar. 2000.
[40] J. E. Colwell, "Vegetation canopy reflectance," *Remote Sens. Environ.*, vol. 3, no. 3, pp. 175–183, 1974.
[41] G. J. Fitzgerald, P. J. Pinter, D. J. Hunsaker, and T. R. Clarke, "Multiple shadow fractions in spectral mixture analysis of cotton canopy," *Remote Sens. Environ.*, vol. 97, no. 4, pp. 526–539, Sep. 2005.
[42] P. J. Zarco-Tejada, J. R. Miller, G. H. Mohammed, T. L. Noland, and P. H. Sampson, "Canopy optical indices from infinite reflectance and canopy reflectance models for forest condition monitoring: Application to hyperspectral CASI data," in *Proc. Int. Geosci. Remote Sens. Symp.*, 1999, pp. 1878–1881.
[43] P. J. Zarco-Tejada, J. R. Miller, G. H. Mohammed, and T. L. Noland, "Chlorophyll fluorescence effects on vegetation apparent reflectance: II. Laboratory and airborne canopy-level measurements with hyperspectral data," *Remote Sens. Environ.*, vol. 74, no. 3, pp. 596–608, Dec. 2000.

Youngkeun Song received the B.S. degree in landscape architecture from the Seoul National University, Seoul, Korea, in 2005 and the M.S. and Ph.D. degrees in global environmental study with a concentration in the landscape ecology and planning from the Kyoto University, Kyoto, Japan, in 2008 and 2012, respectively.

As a part of the study, he was trained in Nakanihon Air Service Company, Ltd., Nagoya, Japan, in 2006, United Nations Environment Programme, Bangkok, Thailand, in 2009, and Asia Air Survey Company, Ltd., Kanagawa, Japan, in 2010. He is currently with the Educational Unit for Studies on the Connectivity of Hilltop, Human and Ocean (CoHHO) at Kyoto University. From the practical experiences. His research involves remote sensing with applications in landscape management strategy.

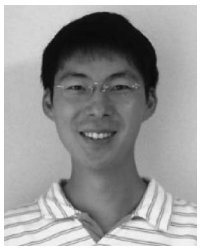

Junichi Imanishi received the M. Landscape Architecture from the University of California, Berkeley, in 2001 and the D. Agri. from Kyoto University, Kyoto, Japan, in 2004.

He is currently an Assistant Professor of the Laboratory of Landscape Ecology and Planning and also an Assistant Professor of Landscape Architecture at Kyoto University. His specialization ranges from remote sensing of vegetation, particularly hyperspectral sensing and laser scanning, to arboriculture and conservation biology.

Hiroshi Hashimoto received the Ph.D. degree in agricultural sciences from Kyoto University, Kyoto, Japan, in 2005.

He is an Assistant Professor of the Laboratory of Landscape Design, Department of Environmental Bioscience, Faculty of Agriculture, Meijo University, Nagoya, Japan. His major theme of study is the conservation of birds in urban and rural areas. He is also interested in the application of remote sensing data to wildlife habitat modeling.

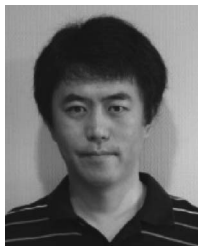

Atsuo Morimura received the Ph.D. degree in agriculture from Osaka Prefecture University, Sakai, Japan, in 1998.

He is currently an Associate Professor of Landscape Ecology with the University of Human Environments, Aichi, Japan. His primary research interest is in the application of remote sensing and GIS to the analysis of human impacts on arid and semiarid land ecosystems.

Yukihiro Morimoto received the Ph.D. degree in agricultural sciences from Kyoto University, Kyoto, Japan, in 1985.

He is a Professor of the Faculty of Bio-Environmental Science, Kyoto Gakuen University, Kameoka, Japan. He previously taught at the Graduate School of Global Environmental Studies of Kyoto University and Osaka Prefecture University since he received his Ph.D. His specialties are conservation and restoration ecology, landscape ecology, and planning.

Dr. Morimoto was the recipient of the Japanese Institute of Landscape Architecture Prize in 1986. Now, he serves as the President of the International Consortium of Landscape and Ecological Engineering, which publishes the journal.

Katsunori Kitada received the B.S. degree in marine science, from Tokai University in 1980.

He is currently the General Manager of the Department of Air Survey and Research, Nakanihon Air Service Company, Ltd., Aichi, Japan. He has contributed to numerous collaborative research works with academic sectors, providing and organizing up-to-date remote sensing data acquired by airborne digital cameras, LiDAR, and hyperspectral sensors.